Chiral iridium(III) complexes with four-membered Ir-S-P-S chelating ring for high-performance circularly polarized OLEDs

Zhi-Ping Yan, Kang Liao, Hua-Bo Han, Jian Su, You-Xuan Zheng,* Jing-Lin Zuo

State Key Laboratory of Coordination Chemistry, Collaborative Innovation Center of Advanced Microstructures, Jiangsu Key Laboratory of Advanced Organic Materials, School of Chemistry and Chemical Engineering, Nanjing University, Nanjing 210093, P. R. China. E-mail: yxzheng@nju.edu.cn

S1. Instruments and details

All experiments were performed under nitrogen atmosphere. The starting reactants and solvents were used as commercial grade without further purifications.

NMR measurements were conducted on a Bruker AM 400 spectrometer. The mass spectra were recorded by Matrix Assisted Laser Desorption Ionization Time of Flight Mass Spectrometry (autoflex TOF/TOF, Bruker Daltonics), High-resolution mass spectra were recorded on a MICROTOF-Q III instrument. Absorption spectra were measured on a UV-3100 spectrophotometer and photoluminescence spectra were obtained from a Hitachi F-4600 photoluminescence spectrophotometer. The absolute photoluminescence quantum yields (Φ) and the decay lifetimes of the complex was measured with HORIBA FL-3 fluorescence spectrometer. Thermogravimetric analysis (TGA) was performed on a Pyris 1 DSC under nitrogen at a heating rate of 10 ^{o}C min^{-1}. The CD and CPL spectra were measured in the same condition with UV-Vis absorption spectra and photoluminescence spectra. The circular dichroism (CD) spectra were measured on a Jasco J-810 circular dichroism spectrometer with 'Low' sensitivity. The scan speed was set as 200 nm/min with 1 nm resolution and a respond time of 1.0 s. The circularly polarized photoluminescence (CPPL) and circularly polarized electroluminescence (CPEL) spectra were measured on a Jasco CPL-300 spectrophotometer based on 'Continuous' scanning mode at 200 nm/min scan speed. The test mode adopts "Slit" mode with the E_x and E_m Slit width 3000 μm and the digital integration time (D.I.T.) is 2.0 s with multiple accumulations (10 times or more).

S2. Experiment Procedures

The $[(C\wedge N)_2Ir(\mu\text{-}Cl)]_2$ chloride-bridged dimmer and ancillary ligands $\mathbf{L_1}$ and $\mathbf{L_2}$ were prepared according to the reported method.[1]

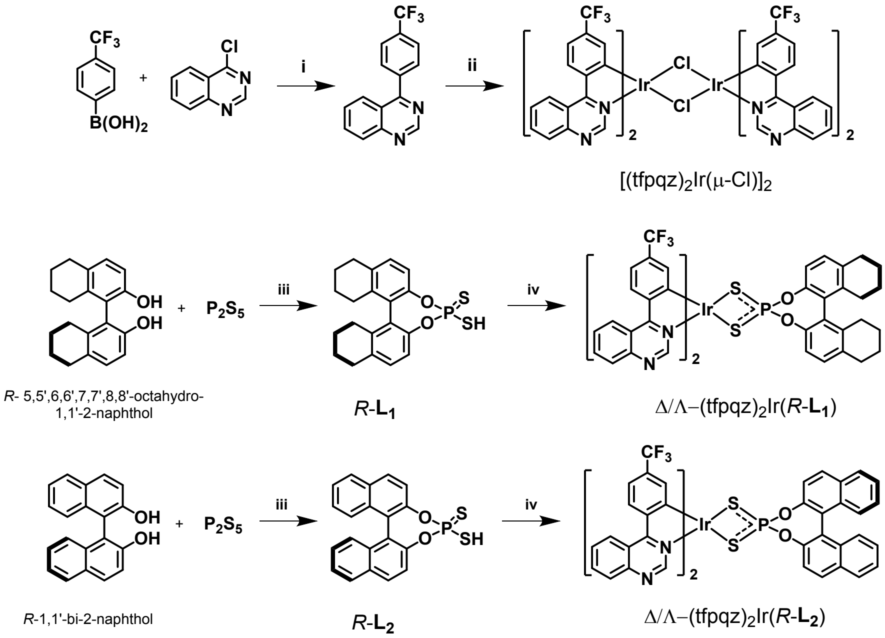

i. Pd(PPh$_3$)$_4$, K$_2$CO$_3$, THF-H$_2$O, 70 °C, 12 h **iii. Toluene, 110 °C**

ii. IrCl$_3$, EtOCH$_2$CH$_2$OH, 115 °C, 12 h **iv. K$_2$CO$_3$, CHCl$_3$, 50°C, 10 min**

Scheme S1. Synthesize procedures of Δ/Λ-(tfpqz)$_2$Ir(*R*-**L$_1$**) and Δ/Λ-(tfpqz)$_2$Ir(*R*-**L$_2$**).

2.1 Preparation of ancillary ligand L$_1$ and L$_2$ enantiomers.

A mixture of (*R*)-5,5',6,6',7,7',8,8'-octahydro-[1,1'-binaphthalene]-2,2'-diol (5.72 g, 0.02 mol) and phosphorus pentasulfide (2.22 g, 0.01 mol) was refluxed in dry toluene (30 mL) for 24 h. Then the solution was cooled down to room temperature and solvent was removed under vacuum. The crude product was purified by column chromatography (silica gel, methanol: dichloromethane 1:20 (v/v)) to get the grey solid 5.2 g (70%) *R*-**L$_1$**. The other enantiopure isomers *S*-**L$_1$**, *R*-**L$_2$** and *S*-**L$_2$** were obtained by similar procedure.

2.2 Preparation of enantiomeric Ir(III) complexes Δ-(tfpqz)$_2$Ir(*R*-L$_1$) and Λ-(tfpqz)$_2$Ir(*R*-L$_1$).

A mixture of *R*-**L$_1$** (0.8 g, 0.79 mmol), K$_2$CO$_3$ (0.1 g, 0.79 mmol) and [(C^N)$_2$Ir(μ-Cl)]$_2$ chloride-bridged dimmer (0.7 g, 1.67 mmol) were added to CHCl$_3$ (15 mL) and heated at 50 °C for 10 min. The solvent was evaporated at low pressure and the crude product was purified by column chromatography (silica gel, dichloromethane: petroleum ether 1:1 (v/v)) to get the luminous orange solid which is the racemic complex Δ/Λ-(tfpqz)$_2$Ir(*R*-**L$_1$**) with 1:1 ratio. And then the racemic complex was further purified by column chromatography (silica gel, ethyl acetate: petroleum ether 1:4 (v/v)) to get the enantiopure isomers Δ-(tfpqz)$_2$Ir(*R*-**L$_1$**) and Λ-(tfpqz)$_2$Ir(*R*-**L$_1$**). The other enantiopure isomers Δ-(tfpqz)$_2$Ir(*S*-**L$_1$**), Λ-(tfpqz)$_2$Ir(*S*-**L$_1$**), Δ-(tfpqz)$_2$Ir(*R*-**L$_2$**), Λ-(tfpqz)$_2$Ir(*R*-**L$_2$**), Δ-(tfpqz)$_2$Ir(*R*-**L$_2$**) and Λ-(tfpqz)$_2$Ir(*R*-**L$_2$**) were prepared in the same way.

Δ/Λ-(tfpqz)$_2$Ir(*R*-**L$_1$**): yield 65%. HR-MS Calculated: 1126.1551 for $C_{50}H_{36}F_6IrN_4O_2PS_2$, found: 1126.1593. MALDI-TOF-MS for Δ-(tfpqz)$_2$Ir(*R*-**L$_1$**), Calculated: 1126.16, founded: 1125.28. ^{1}H NMR (400 MHz, CDCl$_3$) δ 10.41 (s, 2H), 8.84 (d, *J* = 8.6 Hz, 2H), 8.44 (d, *J* = 8.4 Hz, 2H), 8.31 (d, *J* = 8.5 Hz, 2H), 8.04 (t, *J* = 8.4 Hz, 2H), 7.88 (t, *J* = 7.5 Hz, 2H), 7.28-7.19 (m, 2H), 6.87 (d, *J* = 8.3 Hz, 2H), 6.72 (s, 2H), 6.42 (dd, *J* = 8.2, 1.8 Hz, 2H), 2.83-2.70 (m, 4H), 2.64 (ddd, J = 12.7, 8.8, 4.4 Hz, 2H), 2.31-2.20 (m, 2H), 1.82-1.68 (m, 6H), 1.62-1.55 (m, 2H). ^{13}C NMR (100 MHz, CDCl$_3$) δ 174.08, 157.05, 157.04, 154.75, 150.84, 146.86, 146.85, 145.25, 145.12, 138.52, 138.50, 135.83, 135.80, 135.08, 131.94, 131.59, 129.45, 129.35, 129.33, 129.01, 128.30, 128.26, 127.37, 126.92, 126.89, 125.86, 124.65, 121.93, 121.67, 119.21, 119.04, 119.01, 118.84, 118.80, 29.13, 27.84, 22.46, 22.27. MALDI-TOF-MS for Λ-(tfpqz)$_2$Ir(*R*-**L$_1$**), Calculated: 1126.16, founded: 1126.43. ^{1}H NMR (400 MHz, CDCl$_3$) δ 10.53 (s, 2H), 8.82 (d, *J* = 8.5 Hz, 2H), 8.43 (d, *J* = 8.4 Hz, 2H), 8.30 (d, *J* = 8.3 Hz, 2H), 8.00 (t, *J* = 8.5 Hz, 2H), 7.83 (t, *J* = 7.8 Hz, 2H), 7.35-7.20 (m, 4H), 7.14 (d, *J* = 8.3 Hz, 2H), 6.76 (s, 2H), 2.88-2.71 (m, 4H), 2.62 (ddd, *J* = 16.0, 8.4, 4.3 Hz, 2H), 2.26-2.16 (m, 2H), 1.77-1.69 (m, 6H), 1.54-1.44 (m, 2H). ^{13}C NMR (100 MHz, CDCl$_3$) δ 174.02, 156.77, 156.76, 154.60, 150.87, 146.96, 146.95, 145.09, 144.96, 138.52, 138.50, 135.96, 135.93, 135.08, 131.90, 131.62, 129.65, 129.62, 129.42, 129.05, 128.35, 128.32, 127.39, 126.95, 126.93, 125.74, 124.67, 121.95, 121.76, 119.56, 119.53, 118.92, 118.88, 118.85, 29.16, 27.79, 22.46, 22.25.

Δ/Λ-(tfpqz)$_2$Ir(*S*-**L$_1$**): yield 65%. HR-MS Calculated: 1126.1551 for $C_{50}H_{36}F_6IrN_4O_2PS_2$, found: 1126.1623. MALDI-TOF-MS for Δ-(tfpqz)$_2$Ir(*S*-**L$_1$**), Calculated: 1126.16, founded: 1125.41. ^{1}H NMR (400 MHz, CDCl$_3$) δ 10.53 (s, 2H), 8.81 (d, *J* = 8.6 Hz, 2H), 8.43 (d, *J* = 8.4 Hz, 2H), 8.30 (d, *J* = 7.9 Hz, 2H), 8.01 (t, *J* = 8.3 Hz, 2H), 7.84 (t, *J* = 7.8 Hz, 2H), 7.30-7.22 (m, 4H), 7.14 (d, *J* = 8.3 Hz, 2H), 6.76 (s, 2H), 2.88-2.70 (m, 4H), 2.62 (ddd, *J* = 16.2, 8.5, 4.4 Hz, 2H), 2.25-2.16 (m, 2H), 1.80-1.68 (m, 6H), 1.55-1.43 (m, 2H). ^{13}C NMR (100 MHz, CDCl$_3$) δ 174.01, 156.78, 156.77, 154.61, 150.89, 146.97, 146.96, 145.10, 144.98, 138.51, 138.49, 135.95, 135.92, 135.05, 131.88, 131.62, 129.63, 129.61, 129.43, 129.02, 128.36, 128.31, 127.39, 126.95, 126.93, 125.73, 124.67, 121.95, 121.77, 119.57, 119.53, 118.90, 118.86, 118.83, 29.16, 27.79, 22.45, 22.25. MALDI-TOF-MS for Λ-(tfpqz)$_2$Ir(*S*-**L$_1$**), Calculated: 1126.16, founded: 1126.35. ^{1}H NMR (400 MHz, CDCl$_3$) δ 10.41 (s, 2H), 8.87 (d, *J* = 8.5 Hz, 2H), 8.45 (d, *J* = 8.4 Hz, 2H), 8.33 (d, *J* = 8.0 Hz, 2H), 8.05 (t, *J* = 7.1 Hz, 2H), 7.90 (t, *J* = 7.2 Hz, 2H), 7.26-7.21 (m, 2H), 6.87 (d, *J* = 8.3 Hz, 2H), 6.71 (s, 2H), 6.42 (dd, *J* = 8.2, 1.9 Hz, 2H), 2.83-2.70 (m, 4H), 2.64 (ddd, *J* = 16.1, 8.7, 4.4 Hz, 2H), 2.31-2.21 (m, 2H), 1.79-1.71 (m, 6H), 1.62-1.50 (m, 2H). ^{13}C NMR (100 MHz, CDCl$_3$) δ 174.08, 157.07, 157.06, 154.75, 150.85, 146.86, 146.85, 145.26, 145.13, 138.51, 138.49, 135.81, 135.79, 135.04, 131.92, 131.60, 129.47, 129.33, 129.30, 128.98, 128.30, 128.26, 127.37, 126.92, 126.89, 125.85, 124.65, 121.93, 121.68, 119.21, 119.05, 119.01, 118.82, 118.79, 29.13, 27.83, 22.45, 22.26.

Δ/Λ-(tfpqz)$_2$Ir(*R*-**L$_2$**): yield 70%. HR-MS Calculated: 1118.0925 for $C_{50}H_{28}F_6IrN_4O_2PS_2$, found: 1118.1032. MALDI-TOF-MS for Δ-(tfpqz)$_2$Ir(*R*-**L$_2$**), Calculated: 1118.09, founded: 1117.19. ^{1}H NMR (400 MHz, CDCl$_3$) δ 10.46 (s, 2H), 8.88 (d, *J* = 8.6 Hz, 2H), 8.46 (d, *J* = 8.5 Hz, 2H), 8.35 (d, *J* = 8.3 Hz, 2H), 8.06 (t, *J* = 7.6 Hz, 2H), 7.93-7.83 (m, 4H), 7.77 (d, *J* = 8.8 Hz, 2H), 7.46-7.35 (m, 4H), 7.26 (m, 4H), 6.93 (d, *J* = 8.8 Hz, 2H), 6.74 (s, 2H). ^{13}C NMR (100 MHz, CDCl$_3$) δ 174.10, 156.60, 156.58, 154.70, 150.93, 146.87, 146.86, 146.54, 146.40, 135.21, 132.47, 132.45, 132.34, 132.00, 131.82, 131.81, 131.72, 131.40, 130.51, 130.50, 129.51, 129.14, 128.47, 128.34, 128.30, 127.36, 127.17, 126.63, 125.87, 125.75, 124.64, 122.56, 122.53, 121.92, 121.72, 121.40, 121.38, 119.20, 118.99, 118.96. MALDI-TOF-MS for Λ-(tfpqz)$_2$Ir(*R*-**L$_2$**), Calculated: 1118.09, founded: 1117.18 . ^{1}H NMR (400 MHz, CDCl$_3$) δ 10.63 (s, 2H), 8.77 (d, *J* = 8.6 Hz, 2H), 8.41 (d, *J* = 8.4 Hz, 2H), 8.30 (d, *J* = 8.4 Hz, 2H), 8.10-7.94 (m, 4H), 7.91 (d, *J* = 8.2 Hz, 2H), 7.85-7.73 (m, 4H), 7.42 (t, *J* = 7.4 Hz, 2H), 7.33 (d, *J* = 8.5 Hz, 2H), 7.28-7.19 (m, 4H), 6.76 (s, 2H). ^{13}C NMR (100 MHz, CDCl$_3$) δ 174.04, 156.26, 156.25, 154.58, 150.88, 147.00, 147.00, 146.37, 146.24, 135.19, 132.48, 132.46, 132.33, 132.00, 131.89, 131.87, 131.71, 131.40, 130.84, 130.83, 129.40, 129.15, 128.51, 128.33, 128.29, 127.40, 127.09, 126.63, 125.78, 125.73, 124.68, 122.61, 122.58, 121.96, 121.81, 121.78, 121.77, 119.24, 119.04, 119.00.

Δ/Λ-(tfpqz)$_2$Ir(*S*-**L$_2$**): yield 60%. HR-MS Calculated: 1118.0925 for $C_{50}H_{28}F_6IrN_4O_2PS_2$, found: 1118.1063. MALDI-TOF-MS for Δ-(tfpqz)$_2$Ir(*S*-**L$_2$**), Calculated: 1118.09, founded: 1117.32. ^{1}H NMR (400 MHz, CDCl$_3$) δ 10.61 (s, 2H), 8.82 (d, *J* = 8.6 Hz, 2H), 8.44 (d, *J* = 8.4

Hz, 2H), 8.34 (d, *J* = 8.2 Hz, 2H), 8.10-7.97 (m, 4H), 7.94 (d, *J* = 8.1 Hz, 2H), 7.88-7.75 (m, 4H), 7.45 (t, *J* = 7.4 Hz, 2H), 7.35 (d, *J* = 8.5 Hz, 2H), 7.30-7.22 (m, 4H), 6.78 (s, 2H). ^{13}C NMR (100 MHz, $CDCl_3$) δ 174.02, 156.24, 156.23, 154.59, 150.91, 147.01, 147.00, 146.37, 146.24, 135.18, 132.48, 132.46, 132.32, 131.99, 131.89, 131.87, 131.70, 131.39, 130.84, 130.82, 129.42, 129.14, 128.51, 128.33, 128.29, 127.40, 127.10, 126.63, 125.78, 125.73, 124.68, 122.61, 122.58, 121.96, 121.81, 121.78, 121.77, 119.24, 119.03, 119.00. MALDI-TOF-MS for Λ-$(tfpqz)_2$Ir(*S*-**L₂**), Calculated: 1118.09, founded:1117.33. ^{1}H NMR (400 MHz, $CDCl_3$) δ 10.46 (s, 2H), 8.88 (d, *J* = 8.5 Hz, 2H), 8.46 (d, *J* = 8.4 Hz, 2H), 8.35 (d, *J* = 8.3 Hz, 2H), 8.06 (t, *J* = 7.5 Hz, 2H), 7.96-7.82 (m, 4H), 7.77 (d, *J* = 8.8 Hz, 2H), 7.50-7.32 (m, 4H), 7.26 (m, 4H), 6.93 (d, *J* = 8.7 Hz, 2H), 6.74 (s, 2H). ^{13}C NMR (100 MHz, $CDCl_3$) δ 174.11, 156.60, 156.59, 154.68, 150.90, 146.85, 146.85, 146.53, 146.39, 135.22, 132.46, 132.44, 132.34, 132.01, 131.82, 131.80, 131.72, 131.40, 130.51, 130.50, 129.49, 129.14, 128.47, 128.33, 128.30, 127.35, 127.16, 126.63, 125.87, 125.74, 124.63, 122.55, 122.52, 121.91, 121.71, 121.39, 121.37, 119.19, 119.00, 118.96.

S3. NMR spectra

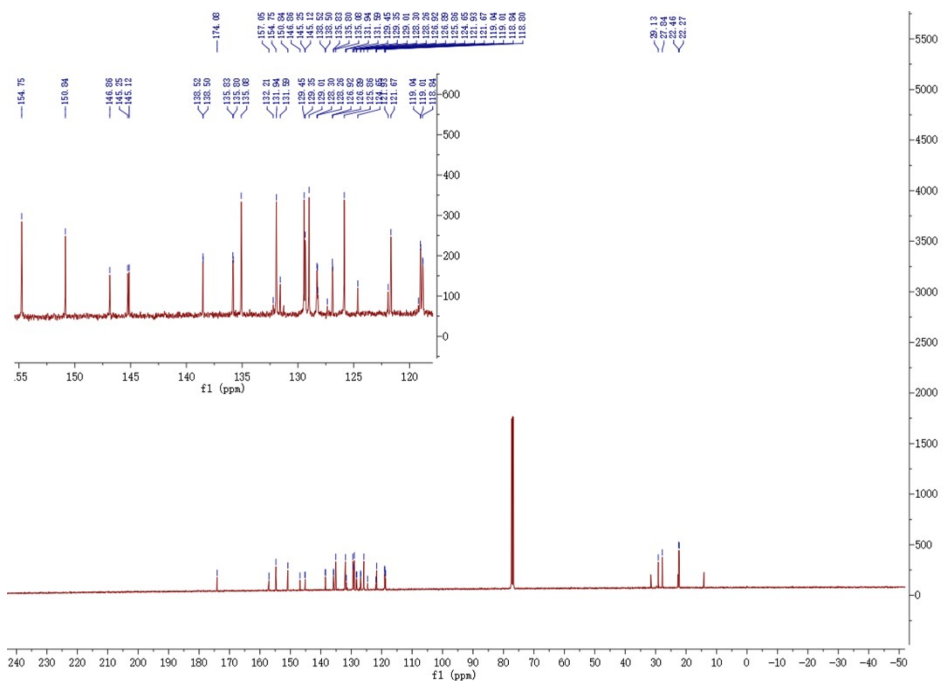

Fig. S1 ^{13}C NMR spectrum (100 MHz, $CDCl_3$) of Δ-$(tfpqz)_2$Ir(*R*-$\mathbf{L_1}$).

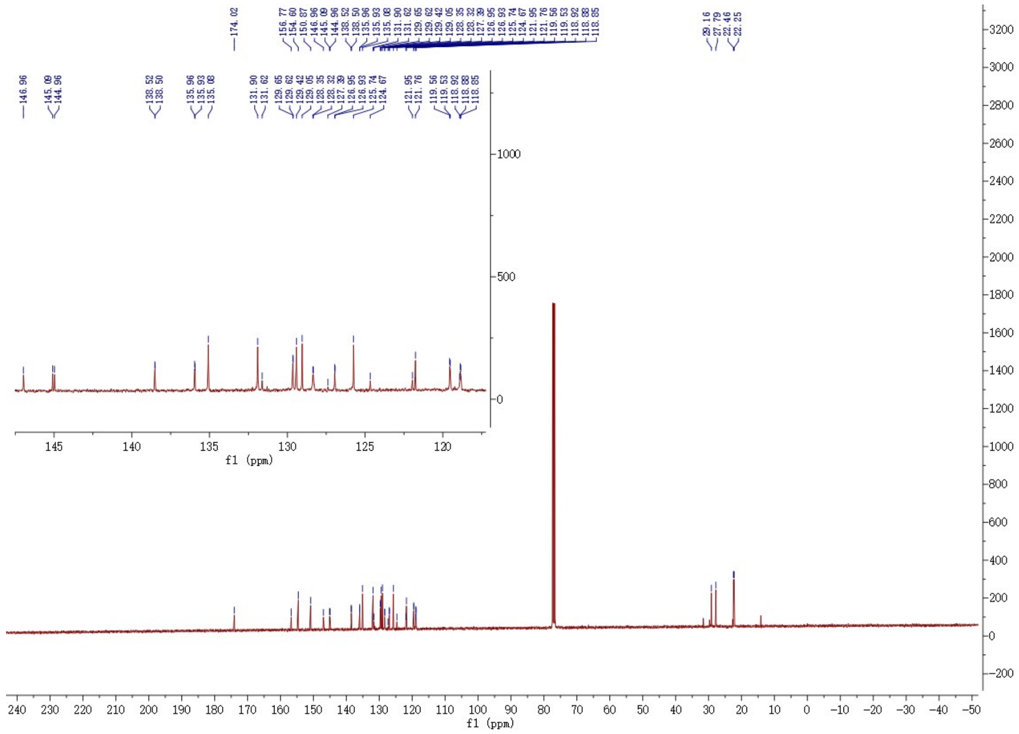

Fig. S2 ^{13}C NMR spectrum (100 MHz, $CDCl_3$) of Λ-$(tfpqz)_2Ir$(*R*-$\mathbf{L_1}$).

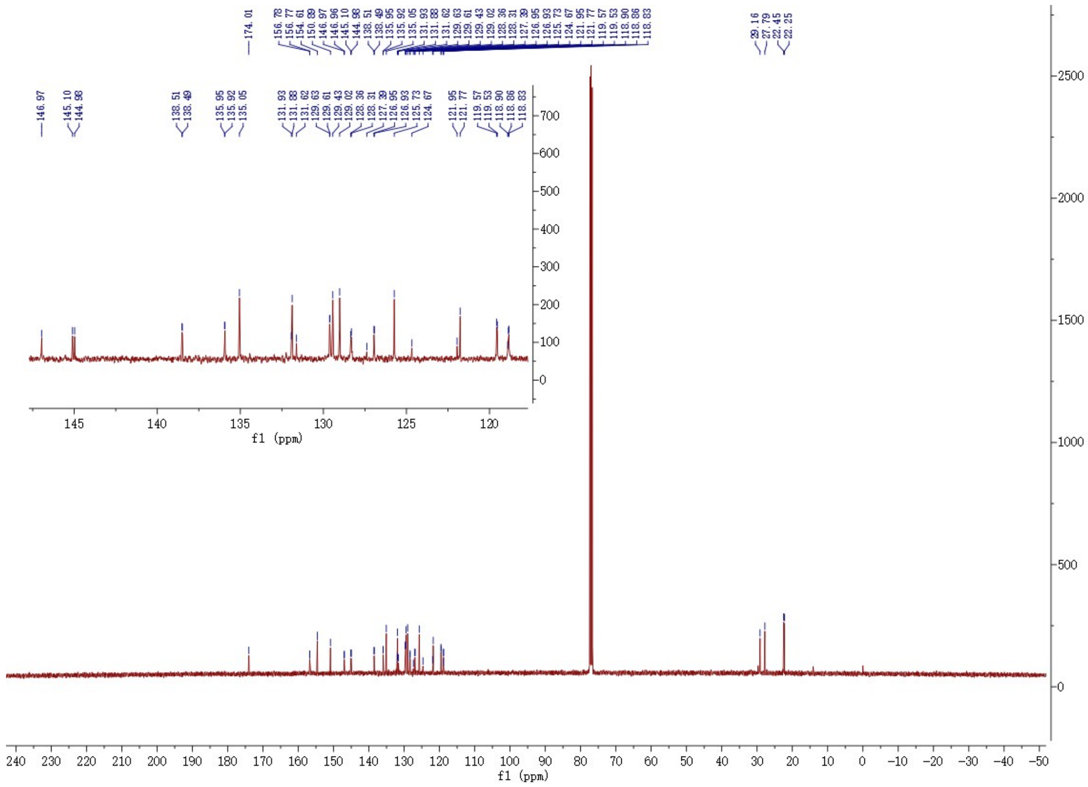

Fig. S3 ^{13}C NMR spectrum (100 MHz, $CDCl_3$) of Δ-$(tfpqz)_2Ir$(*S*-$\mathbf{L_1}$).

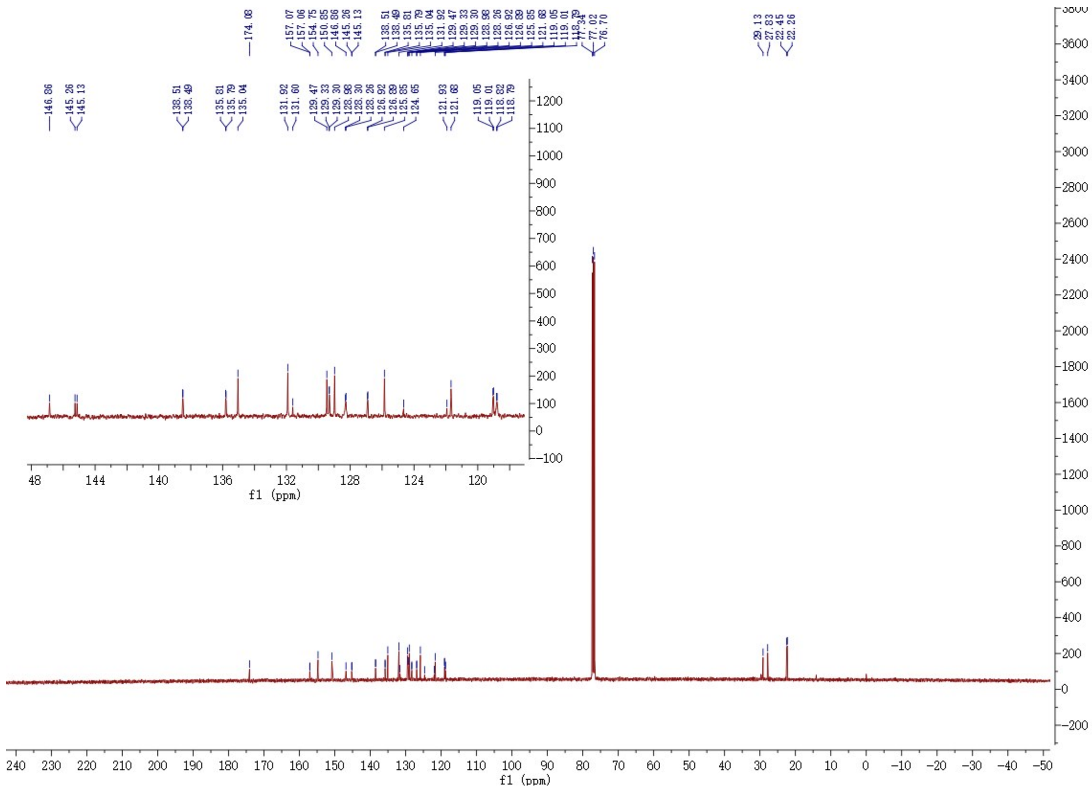

Fig. S4 ^{13}C NMR spectrum (100 MHz, $CDCl_3$) of Λ-$(tfpqz)_2Ir$(*S*-$\mathbf{L_1}$).

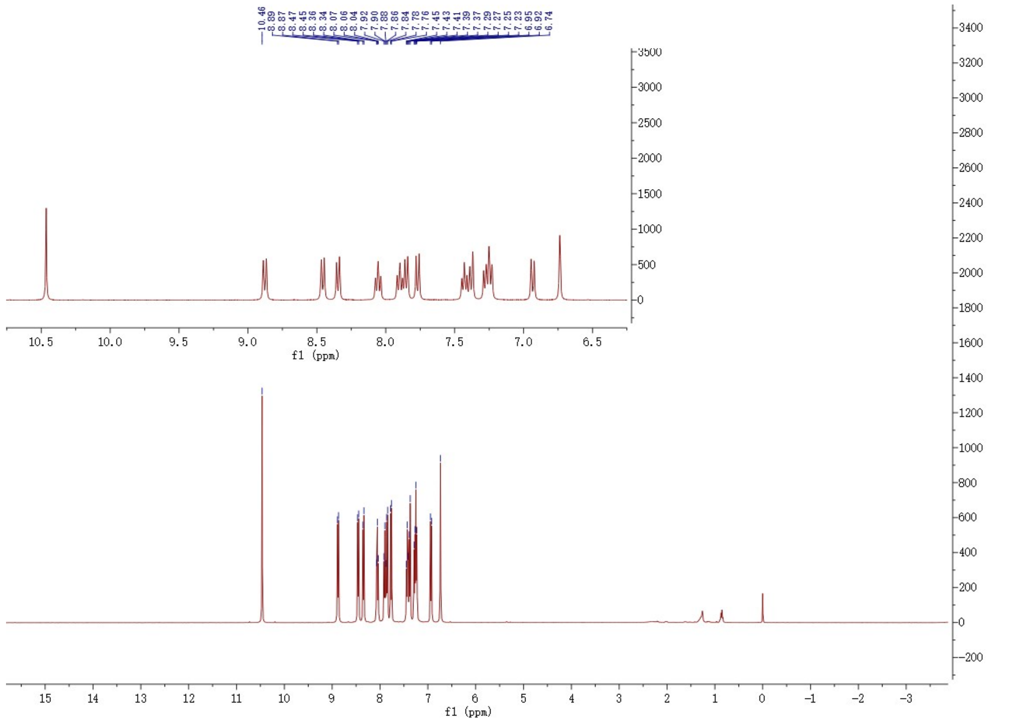

Fig. S5 ^{1}H NMR spectrum (400 MHz, $CDCl_3$) of Δ-$(tfpqz)_2Ir$(*R*-$\mathbf{L_2}$).

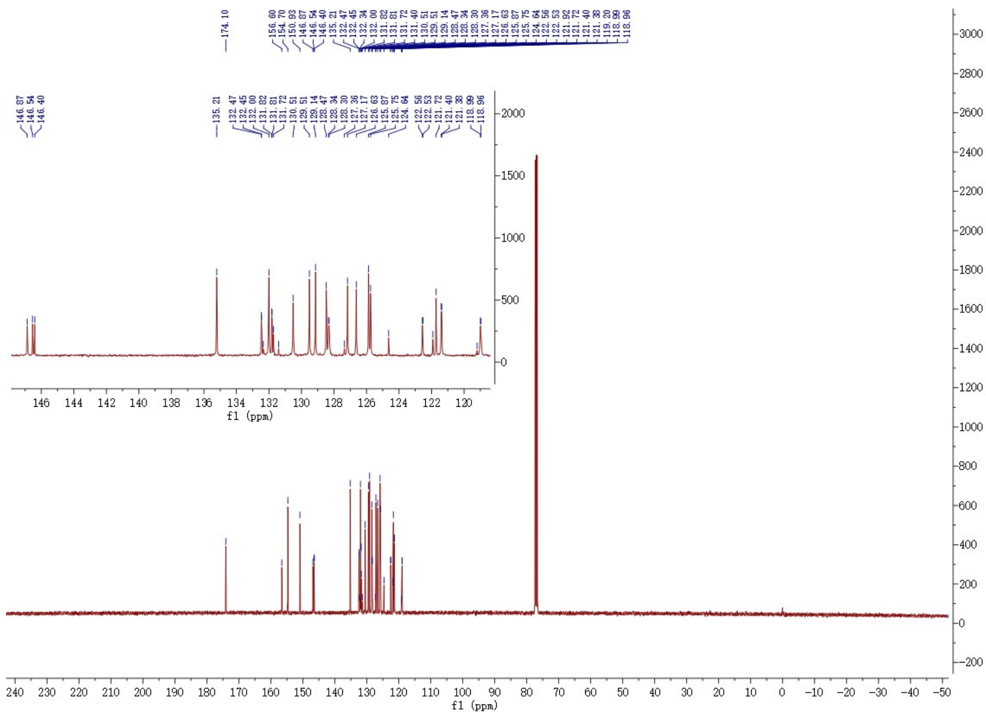

Fig. S6 ^{13}C NMR spectrum (100 MHz, $CDCl_3$) of Δ-$(tfpqz)_2Ir$(*R*-$\mathbf{L_2}$).

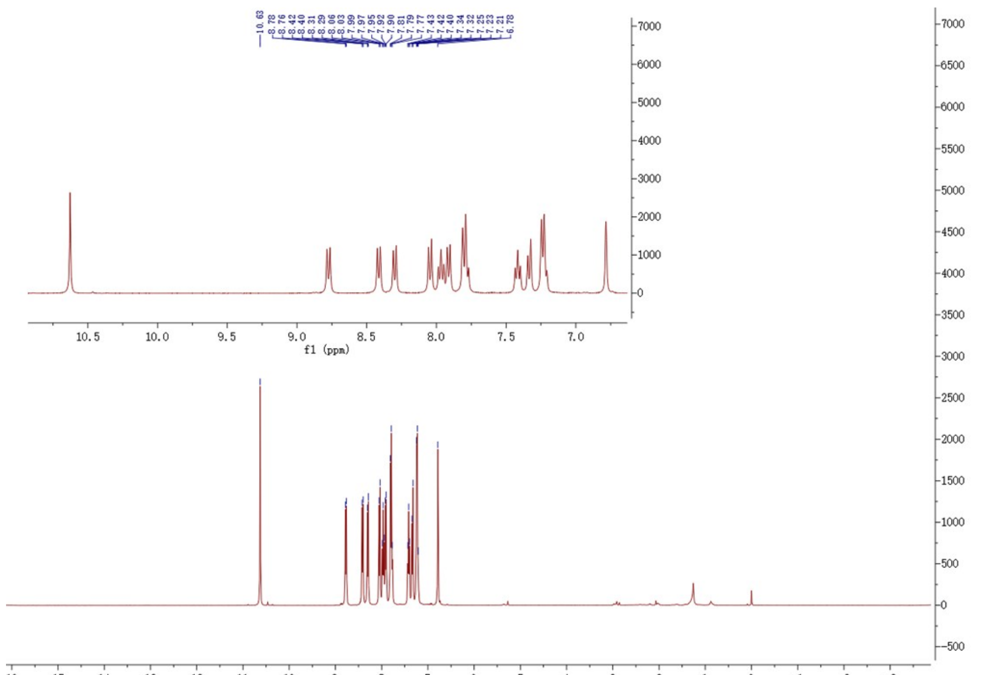

Fig. S7 ^{1}H NMR spectrum (400 MHz, $CDCl_3$) of Λ-$(tfpqz)_2Ir$(*R*-$\mathbf{L_2}$).

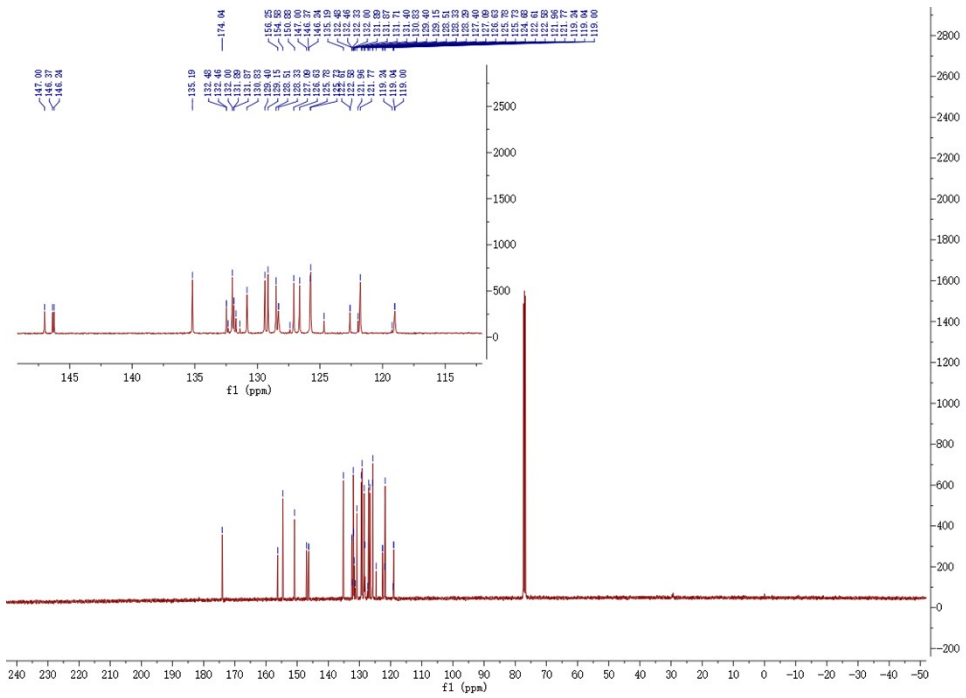

Fig. S8 ^{13}C NMR spectrum (100 MHz, $CDCl_3$) of Λ-$(tfpqz)_2Ir$(*R*-$\mathbf{L_2}$).

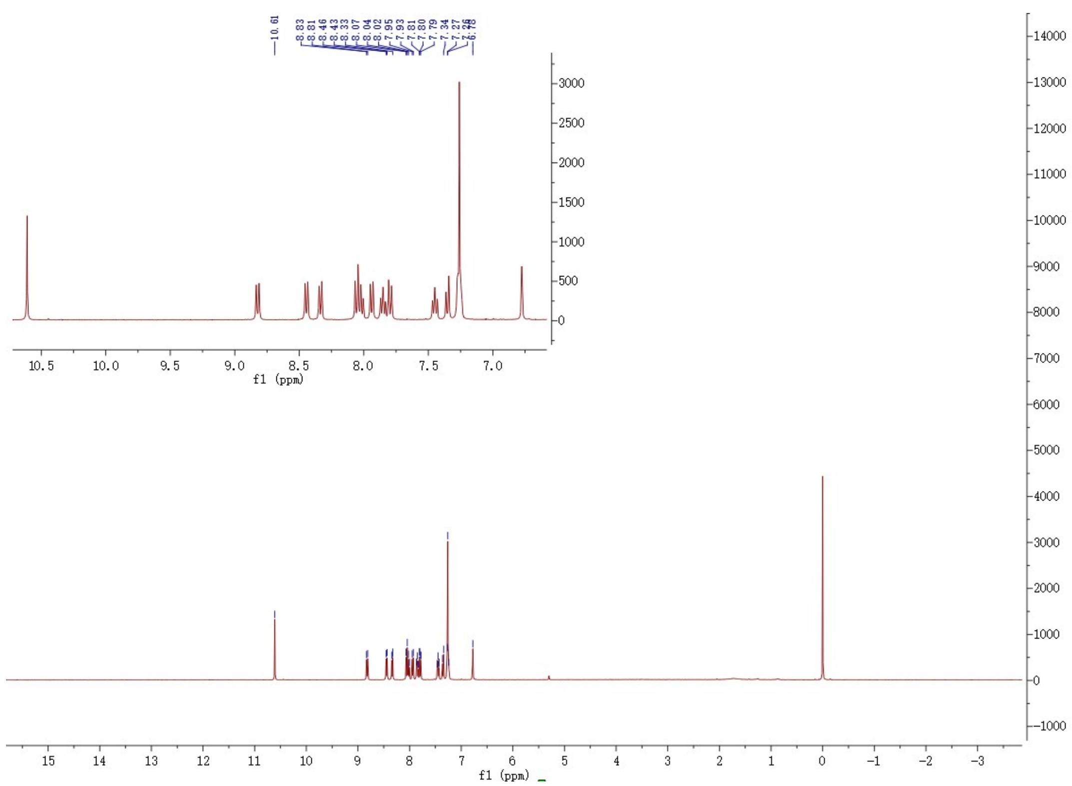

Fig. S9 ^{1}H NMR spectrum (400 MHz, $CDCl_3$) of Δ-$(tfpqz)_2Ir$(*S*-$\mathbf{L_2}$).

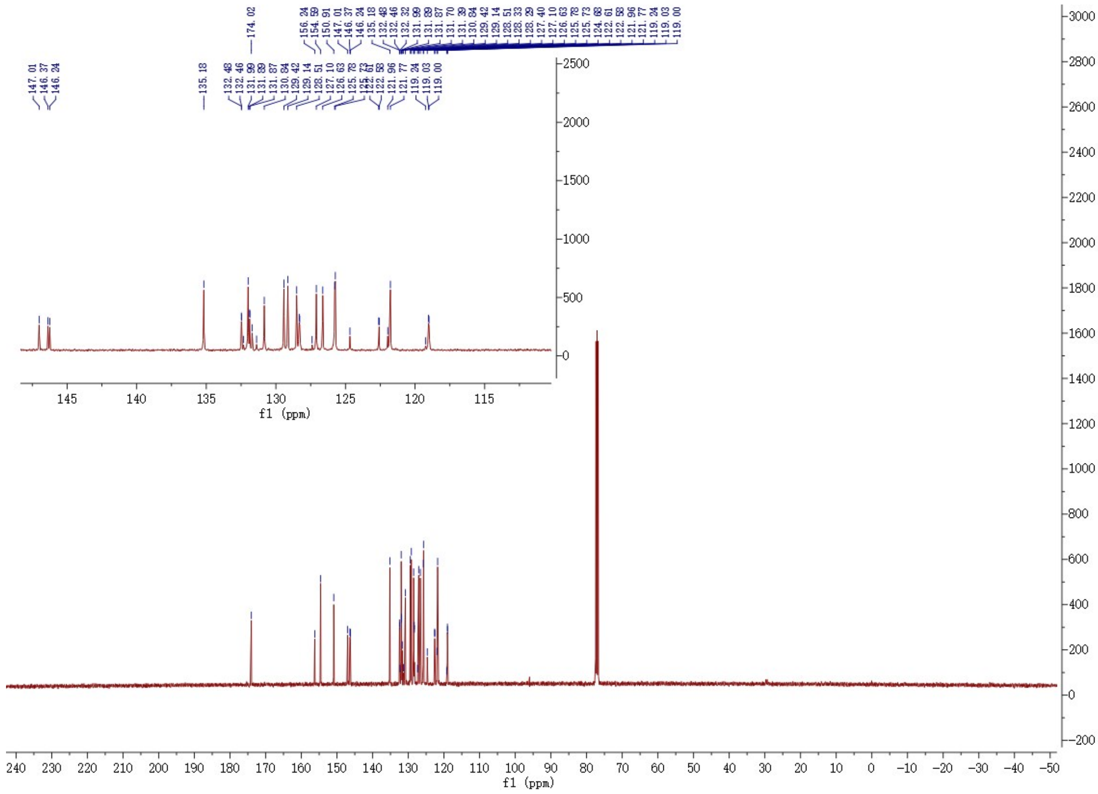

Fig. S10 ^{13}C NMR spectrum (100 MHz, $CDCl_3$) of Δ-$(tfpqz)_2Ir$(*S*-$\mathbf{L_2}$).

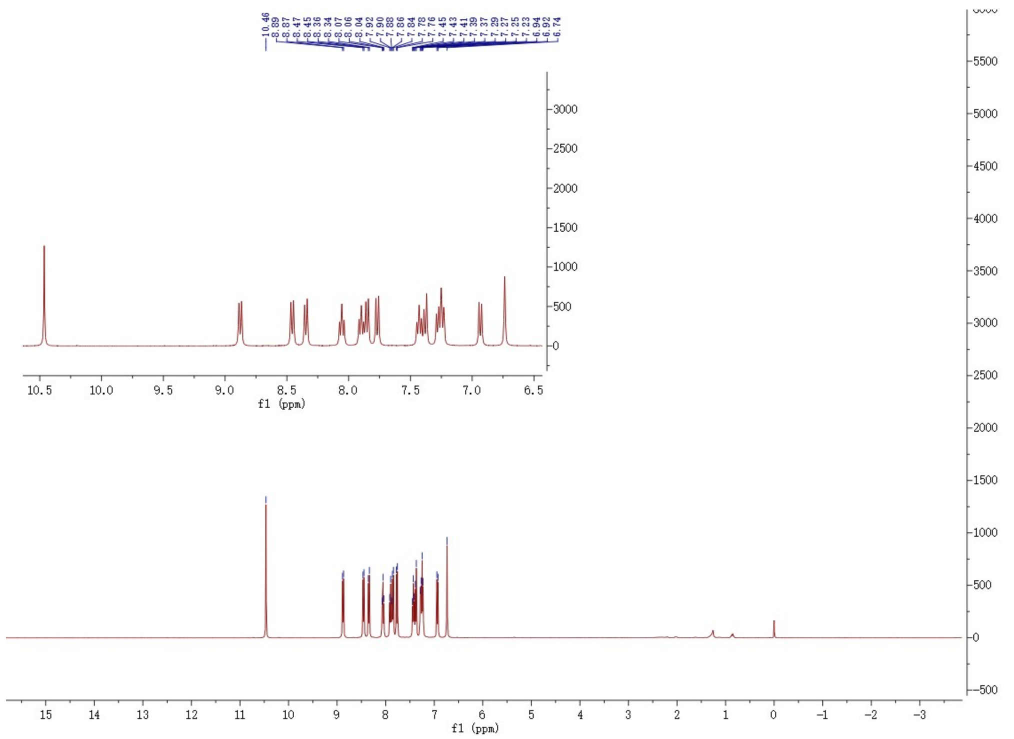

Fig. S11 ^{1}H NMR spectrum (400 MHz, $CDCl_3$) of Λ-$(tfpqz)_2Ir$(*S*-$\mathbf{L_2}$).

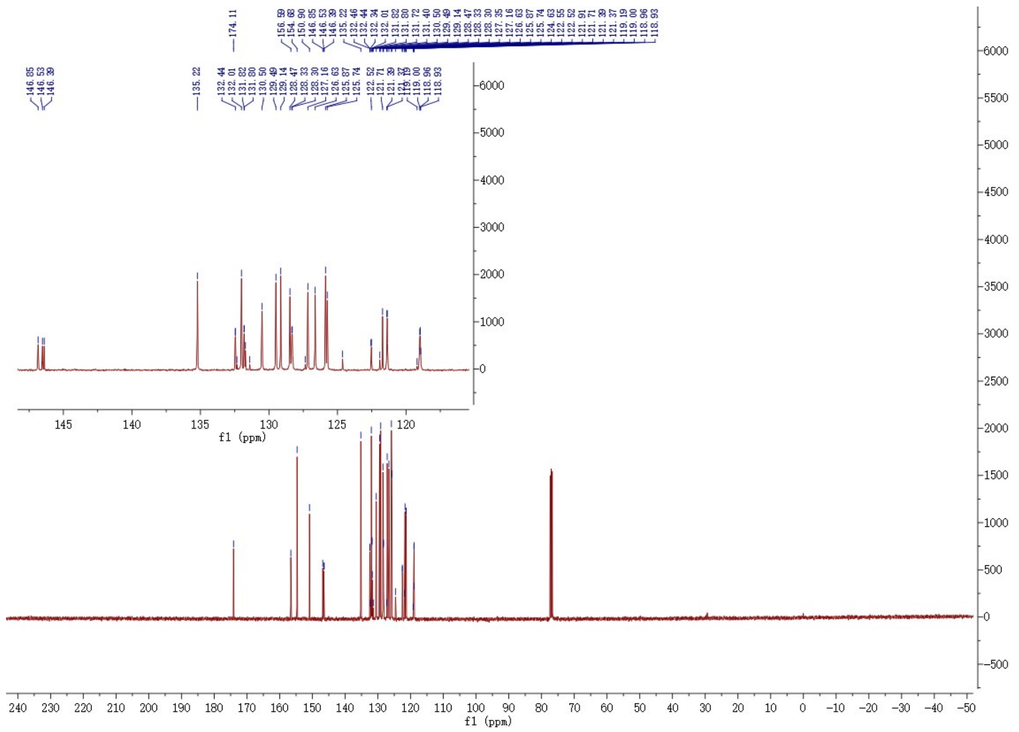

Fig. S12 ^{13}C NMR spectrum (100 MHz, $CDCl_3$) of Λ-$(tfpqz)_2Ir$(*S*-$\mathbf{L_2}$).

S4. X-ray crystallographic data

Table S1. Crystal data and structure refinement for Δ-$(tfpqz)_2$Ir(R-$\mathbf{L_1}$), Λ-$(tfpqz)_2$Ir(S-$\mathbf{L_1}$), Δ-$(tfpqz)_2$Ir(R-$\mathbf{L_2}$), Λ-$(tfpqz)_2$Ir(S-$\mathbf{L_2}$).

Identification code	Δ-$(tfpqz)_2$Ir(R-$\mathbf{L_1}$)	Λ-$(tfpqz)_2$Ir(S-$\mathbf{L_1}$)	Δ-$(tfpqz)_2$Ir(R-$\mathbf{L_2}$)	Λ-$(tfpqz)_2$Ir(S-$\mathbf{L_2}$)
CCDC	1913548	1913549	1913550	1913551
Empirical formula	$C_{50.04}H_{35.42}F_6IrN_4O_2PS_2$	$C_{50}H_{36}F_6IrN_4O_2PS_2$	$C_{50}H_{28}F_6IrN_4O_2PS_2$	$C_{50}H_{28}F_6IrN_4O_2PS_2$
Formula weight	1126.07	1126.18	1118.12	1118.12
Temperature/K	192.98	296.15	296.15	296.15
Crystal system	Monoclinic	Monoclinic	Orthorhombic	Orthorhombic
Space group	$P2_1$	$P2_1$	$P2_12_12_1$	$P2_12_12_1$
a/Å	9.0479(9)	9.0612(5)	11.0991(11)	11.1820(6)
b/Å	10.7246(11)	10.7892(6)	15.4078(16)	15.6943(8)
c/Å	25.204(3)	25.3691(14)	31.051(3)	30.6950(16)
α/°	90	90	90	90
β/°	98	98	90	90
γ/°	90	90	90	90
Volume/$Å^3$	2421.3(4)	2457.6(2)	5310.1(9)	5386.8(5)
Z	2	2	4	4
$\rho_{calc}g/cm^3$	1.545	1.52	1.398	1.3786
μ/mm^{-1}	4.798	2.889	2.683	2.645
F(000)	1115	1115	2197	2197
Theta range for data collection/ deg	2.147 to 26.99	1.62 to 24.99	1.31 to 27.54	1.46 to 27.49
Index ranges	$-10 \le h \le 10, -12 \le k \le 12, -30 \le l \le 17$	$-11 \le h \le 11, -13 \le k \le 14, -25 \le l \le 32$	$0 \le h \le 14, 0 \le k \le 20, 0 \le l \le 40$	$0 \le h \le 14, 0 \le k \le 20, 0 \le l \le 39$
Reflections collected	16720	16988	6759	6824
Independent reflections	7820 [R_{int} = 0.0557]	7978 [R_{int} = 0.0411]	6759 [R_{int} = 0]	6824 [R_{int} =0]
Data/restraints/parameters	7820/2456/655	7978/81/595	6759/14/595	6824/1/595
Goodness-of-fit on F^2	1.025	0.9963	1.02	0.9142
Final R indexes [I>=2σ (I)]	R_1 = 0.0456, wR_2 = 0.1140	R_1 = 0.0435, wR_2 = 0.0940	R_1 = 0.0525, wR_2 = 0.1385	R_1 = 0.0434, wR_2 = 0.0971
Final R indexes [all data]	R_1 = 0.0513, wR_2 = 0.1188	R_1 = 0.0567, wR_2 = 0.0997	R_1 = 0.0697, wR_2 = 0.1479	R_1 = 0.0760, wR_2 = 0.1077
Largest diff. peak/hole / e $Å^{-3}$	0.82/-1.20	0.86/-0.71	1.22/-1.24	1.31/-2.19

$R_1^a = \Sigma||F_o| - |F_c||/\Sigma F_o|$. $wR_2^b = [\Sigma w(F_o^2 - F_c^2)^2/\Sigma w(F_o^2)]^{1/2}$

S5. Photophysical and chiroptical measurement

The 3D excitation-emission correlation spectra of Δ/Λ-(tfpqz)$_2$Ir(R-**L$_1$**) and Δ/Λ-(tfpqz)$_2$Ir(R-**L$_2$**) were measured in CH_2Cl_2 solution at a concentration of 5×10^{-6} mol/L under 298 K. Sample for emission measurement were contained within quartz cuvettes of 1 cm pathlength. Degassing was achieved by three freeze-pump-thaw cycles whilst connected to the vacuum manifold. And the phosphorescence lifetime and absolute quantum yields were measured under an argon atmosphere.

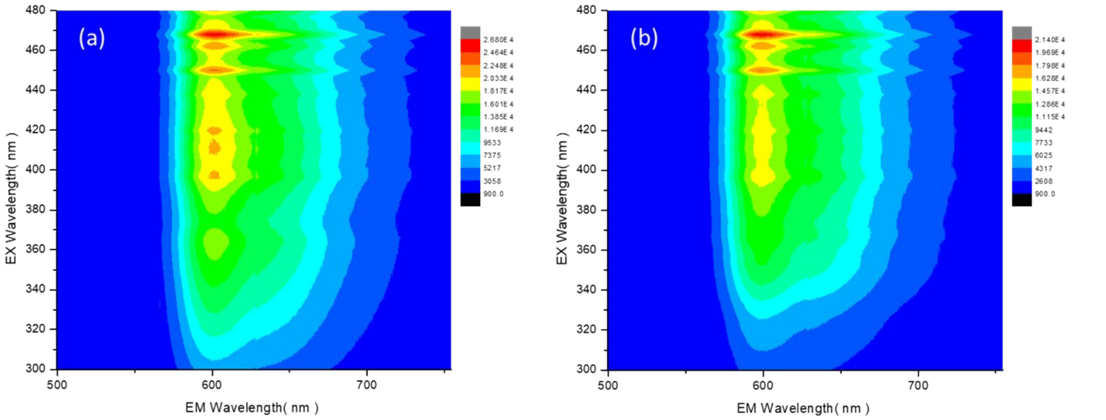

Fig. S13 3D excitation-emission correlation spectra of (a) Δ/Λ-(tfpqz)$_2$Ir(R/S-**L$_1$**) and (b) Δ/Λ-(tfpqz)$_2$Ir(R/S-**L$_2$**).

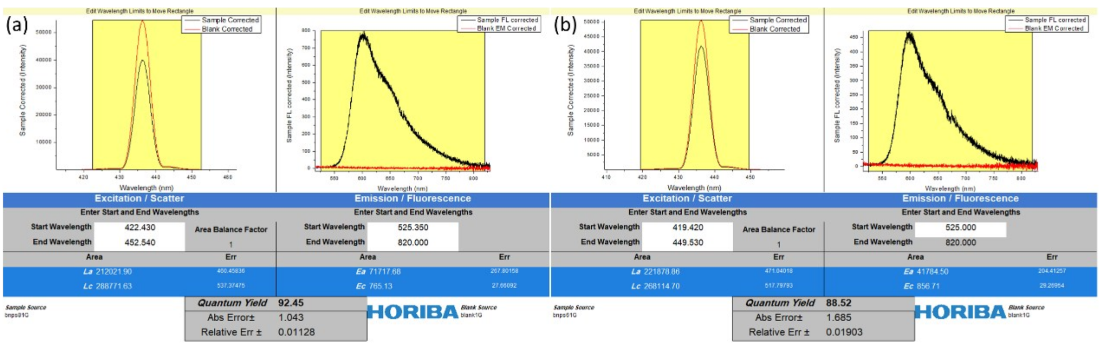

Fig. S14 Absolute photoluminescence quantum yields of (a) Δ/Λ-(tfpqz)$_2$Ir(R/S-**L$_1$**) and (b) Δ/Λ-(tfpqz)$_2$Ir(R/S-**L$_2$**).

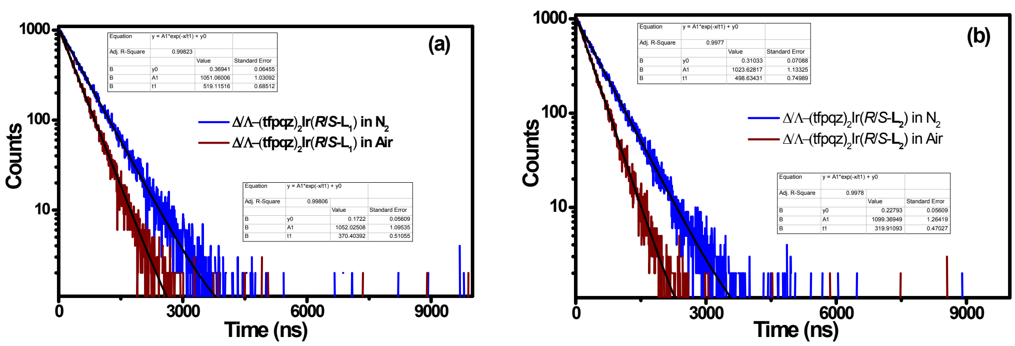

Fig. S15 Transient PL decay spectra of (a) Δ/Λ-(tfpqz)$_2$Ir(R/S-**L$_1$**) and (b) Δ/Λ-(tfpqz)$_2$Ir(R/S-**L$_2$**) in N_2 and air.

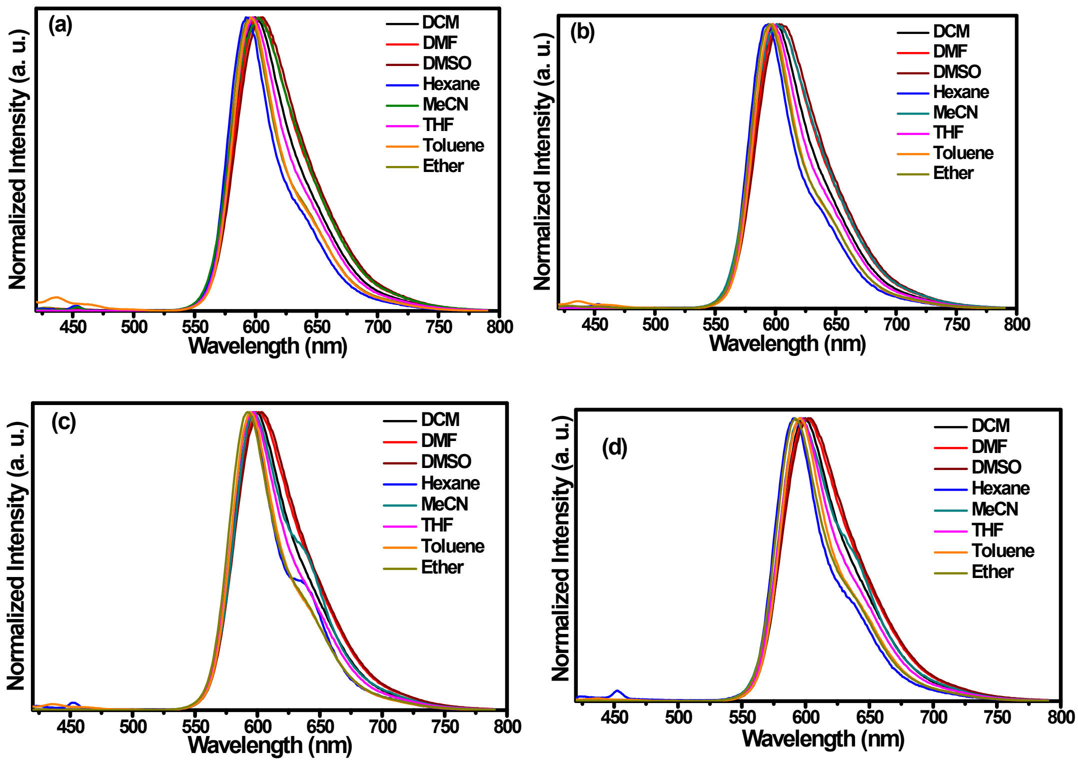

Fig. S16 Normalized PL spectra of (a) Δ/Λ-$(tfpqz)_2$Ir(*R*/*S*-$\mathbf{L_1}$) (new preparation) and (b) Δ/Λ-$(tfpqz)_2$Ir(*R*/*S*-$\mathbf{L_1}$) (after 24 h deposition); (c) Δ/Λ-$(tfpqz)_2$Ir(*R*/*S*-$\mathbf{L_2}$) (new preparation) and (d) Δ/Λ-$(tfpqz)_2$Ir(*R*/*S*-$\mathbf{L_2}$) (after 24 h deposition).

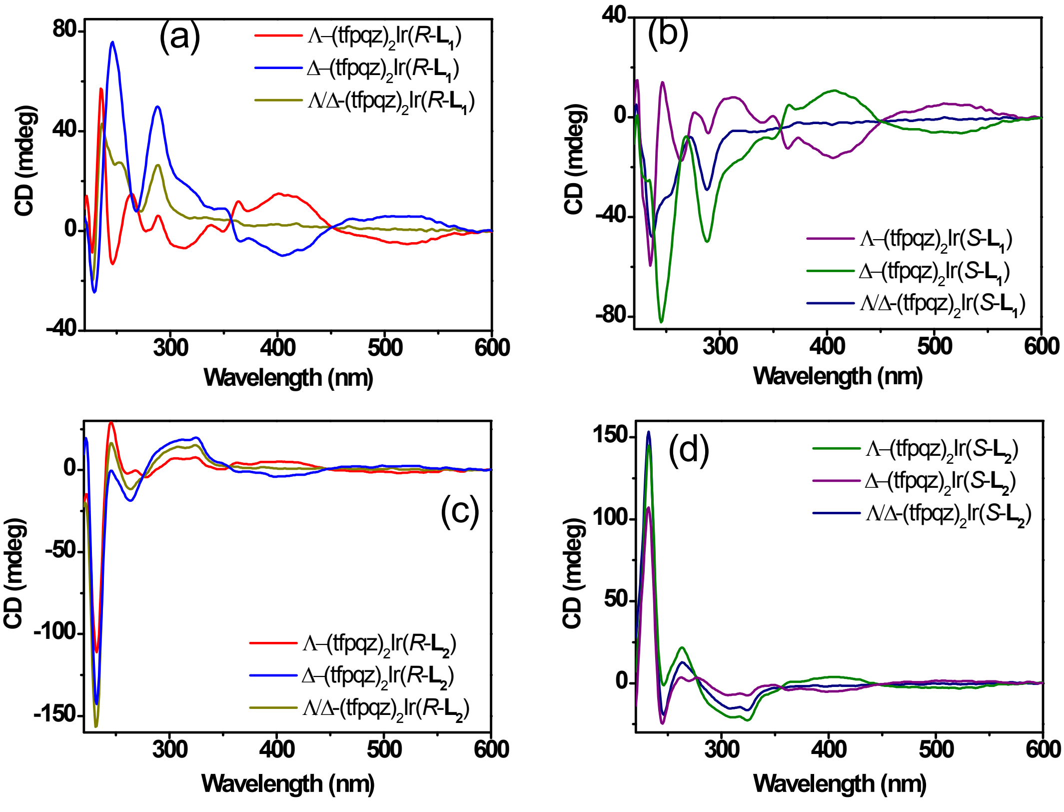

Fig. S17 ECD spectra for the stereoisomers and enantiomeric monomers of (a) Δ/Λ-$(tfpqz)_2$Ir(*R*/*S*-$\mathbf{L_1}$) and (b) Δ/Λ-$(tfpqz)_2$Ir(*R*/*S*-$\mathbf{L_2}$).

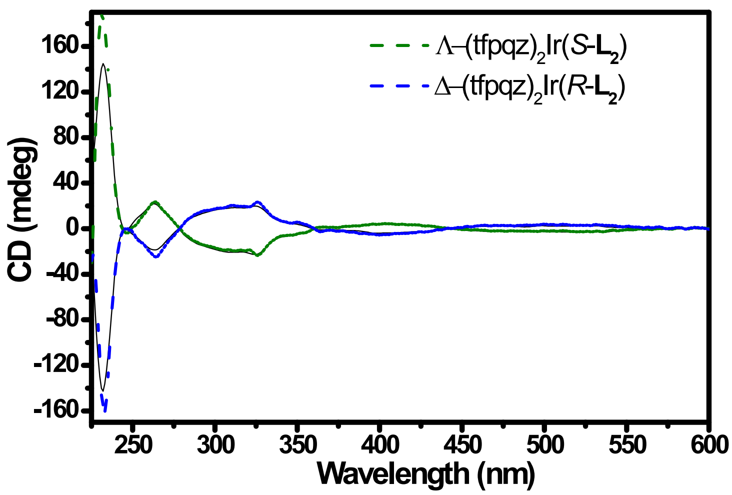

Fig. S18 ECD spectra for Δ-$(tfpqz)_2$Ir(R-$\mathbf{L_2}$) and Λ-$(tfpqz)_2$Ir(S-$\mathbf{L_2}$) after device fabrication (dash).

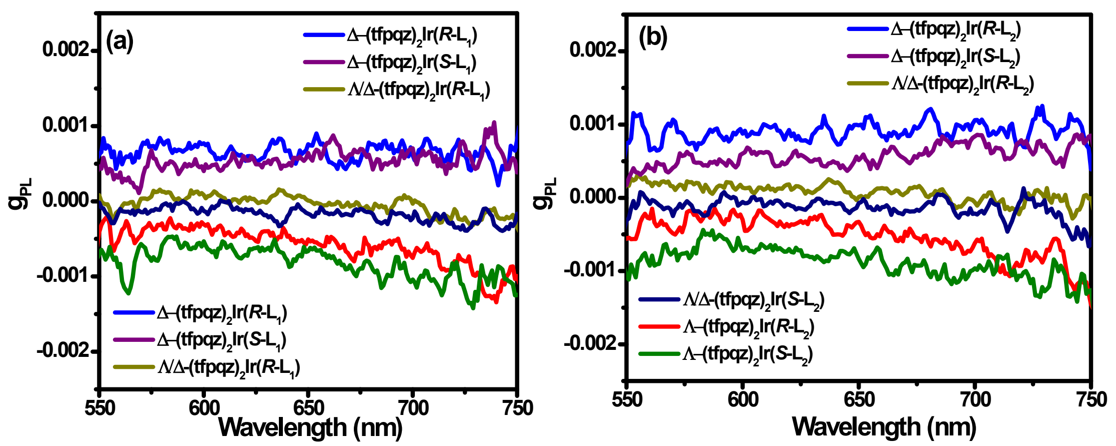

Fig. S19 g_{PL} curves of the stereoisomers and enantiomeric monomers of (a) Δ/Λ-$(tfpqz)_2$Ir(R/S-$\mathbf{L_1}$) and (b) Δ/Λ-$(tfpqz)_2$Ir(R/S-$\mathbf{L_2}$).

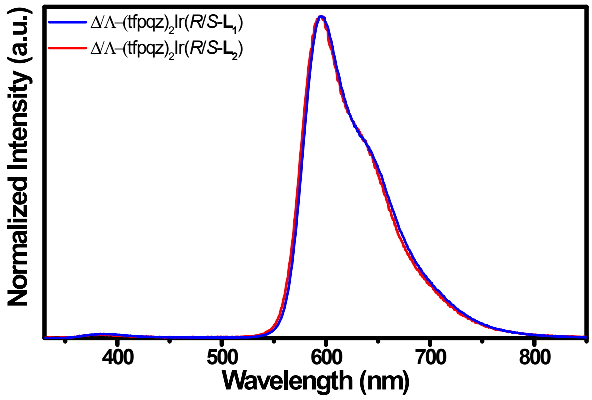

Fig. S20 PL spectra of Δ/Λ-(tfpqz)$_2$Ir(*R*/*S*-**L$_1$**) and Δ/Λ-(tfpqz)$_2$Ir(*R*/*S*-**L$_2$**)in doped film (4 wt% in 26DCzPPy).

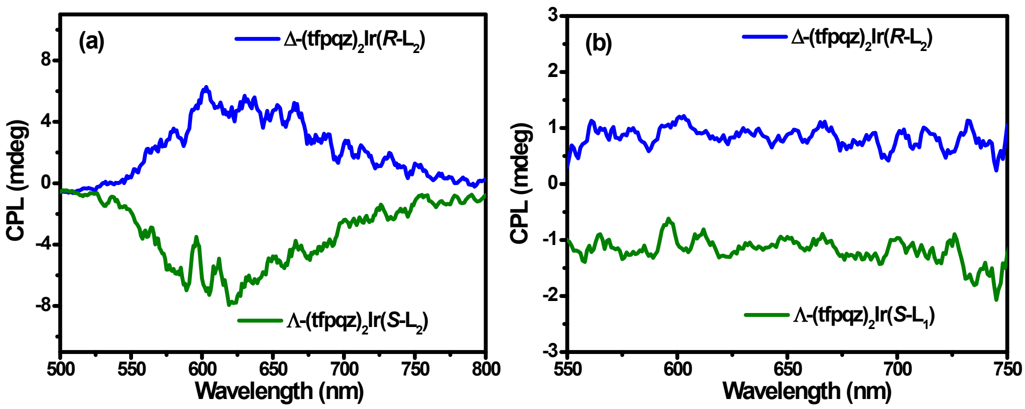

Fig. S21 (a) CPL spectra and (b) g_{PL} curves of Δ-(tfpqz)$_2$Ir(*R*-**L$_2$**) and Λ-(tfpqz)$_2$Ir(*S*-**L$_2$**) in doped film (4 wt% in 26DCzPPy).

Table S2. Photophysical and chiroptical properties for all the isomers.

Complete racemic complex	Compound	λ_{abs} nm	Emission 298 K		Emission 77 K		g_{PL} (10^{-3})		Φ	τ µs
			λ_{PL} nm	FWHM nm	λ_{PL} nm	FWHM nm	solution	flim		
Δ/Λ-(tfpqz)$_2$Ir(*R*/*S*-**L$_1$**)	Δ-(tfpqz)$_2$Ir(*R*-**L$_1$**)	225, 280, 412	597	57	607	36	0.7	-	0.92	0.52
	Λ-(tfpqz)$_2$Ir(R-**L$_1$**)	224, 280, 413	597	57	605	31	-0.4	-		
	Δ-(tfpqz)$_2$Ir(*S*-**L$_1$**)	226, 281, 410	598	57	606	32	0.5	-		
	Λ-(tfpqz)$_2$Ir(*S*-**L$_1$**)	225, 280, 411	599	56	607	35	-0.6	-		
Δ/Λ-(tfpqz)$_2$Ir(*R*/*S*-**L$_2$**)	Δ-(tfpqz)$_2$Ir(*R*-**L$_2$**)	231, 282, 406	601	55	606	34	0.9	1.1	0.88	0.50
	Λ-(tfpqz)$_2$Ir(*R*-**L$_2$**)	233, 282, 405	599	56	607	34	-0.4	-		
	Δ-(tfpqz)$_2$Ir(*S*-**L$_2$**)	231, 283, 407	600	55	607	31	0.5	-		

Λ-(tfpqz)$_2$Ir(*S*-**L**$_2$)	232, 282, 406	602	54	605	34	-0.8	-1.1

S6. Electrochemical measurement and theoretical calculation

Cyclic-voltammetry measurement system at room temperature in deaerated CH_3CN, employing a polished Pt plate as the working electrode, and tetra-*n*-butylammonium perchlorate (0.1M) as the supporting electrolyte, Fc^+/Fc was used as the reference, with the scan rate of 0.1 V/s. The energy levels were calculated using the following equations: E_{HOMO} = - (4.8 + E_{ox}) eV, $E_{LUMO} = E_{HOMO} + E_g$, E_g were calculated from the UV-vis spectra.

All the DFT and TD-DFT calculations were carried out using Gaussian 16 software package. The initial structures were created according to the crystal structure. The ground state geometry optimizations with frequent calculations for all the complexes were performed using B3LYP exchange-correlation functional. On the basis of the optimized structures, vertical transition energy calculations were carried out with m06x functional. For all the calculations, a combination of basis sets that Lanl2dz for platinum and 6-31G (d,p) for the others were employed and the solvent effect are considered by C-PCM model in CH_2Cl_2.

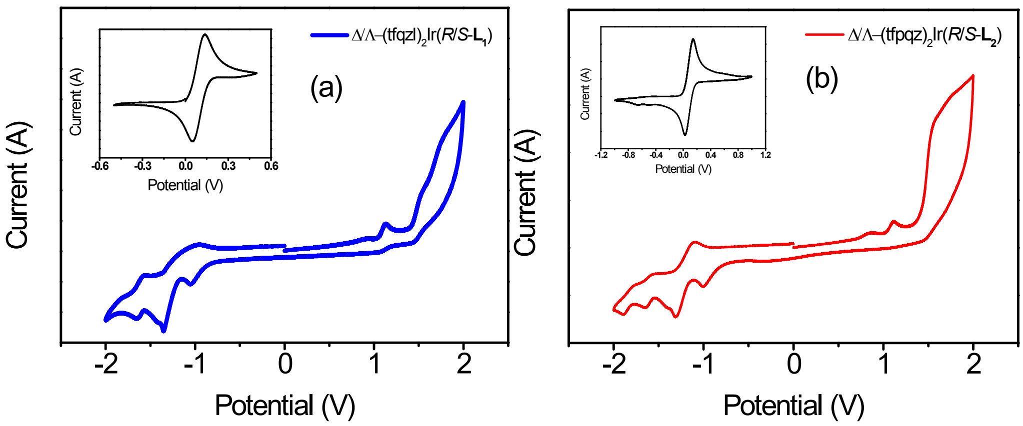

Fig. S22 (a) The cyclic voltammogram curve of (a) Δ/Λ-(tfpqz)$_2$Ir(*R*/*S*-**L**$_1$) and (b) Δ/Λ-(tfpqz)$_2$Ir(*R*/*S*-**L**$_2$).

Table S3. Electrochemical properties of the racemic Ir(III) complexes Δ/Λ-(tfpqz)$_2$Ir(*R*/*S*-**L**$_1$) and Δ/Λ-(tfpqz)$_2$Ir(*R*/*S*-**L**$_2$).

Complex	$E_{ox,onset\ (Ir)}$[a] V	$E_{ox,onset\ (Fe)}$[b] V	$E_{g,opt}$[c] eV	E_{HOMO}[d] eV	E_{LUMO}[e] eV

Δ/Λ-(tfpqz)$_2$Ir(*R*/*S*-**L$_1$**)	1.13	0.13	2.10	-5.80	-3.70
Δ/Λ-(tfpqz)$_2$Ir(*R*/*S*-**L$_2$**)	1.11	0.09	2.12	-5.82	-3.70

[a]: The onset of oxidation curves of racemic Ir(III) complexes; [b]: The onset of oxidation curves of Ferrocene; [c]: Optical gap (= 1240/λ_{onset}); [d]: E_{HOMO} = -[E_{ox} - $E_{(Fc/Fc+)}$ + 4.8] eV; [e]: E_{LUMO} = E_{HOMO} + E_g.

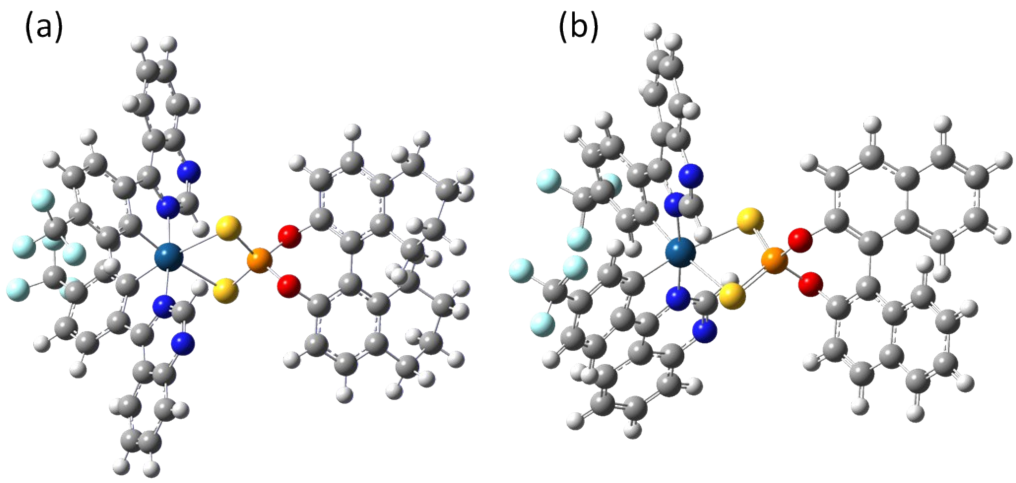

Fig. S23 (a) The geometry optimization of Δ-(tfpqz)$_2$Ir(*R*-**L$_1$**) and Λ-(tfpqz)$_2$Ir(*S*-**L$_2$**).

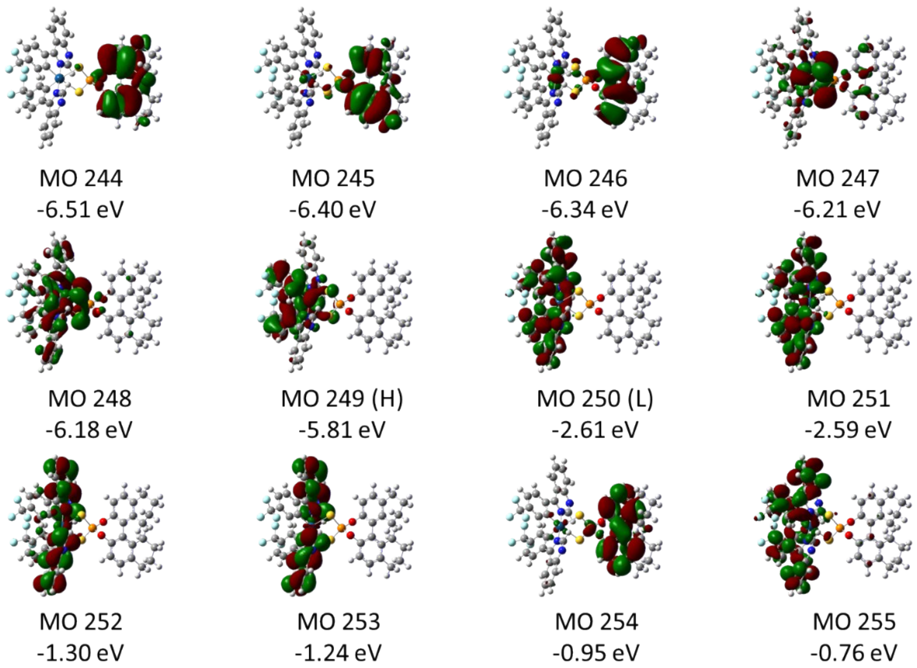

Fig. S24 Electronic clouds distribution of Δ-(tfpqz)$_2$Ir(*R*-**L$_1$**) in selected transitions.

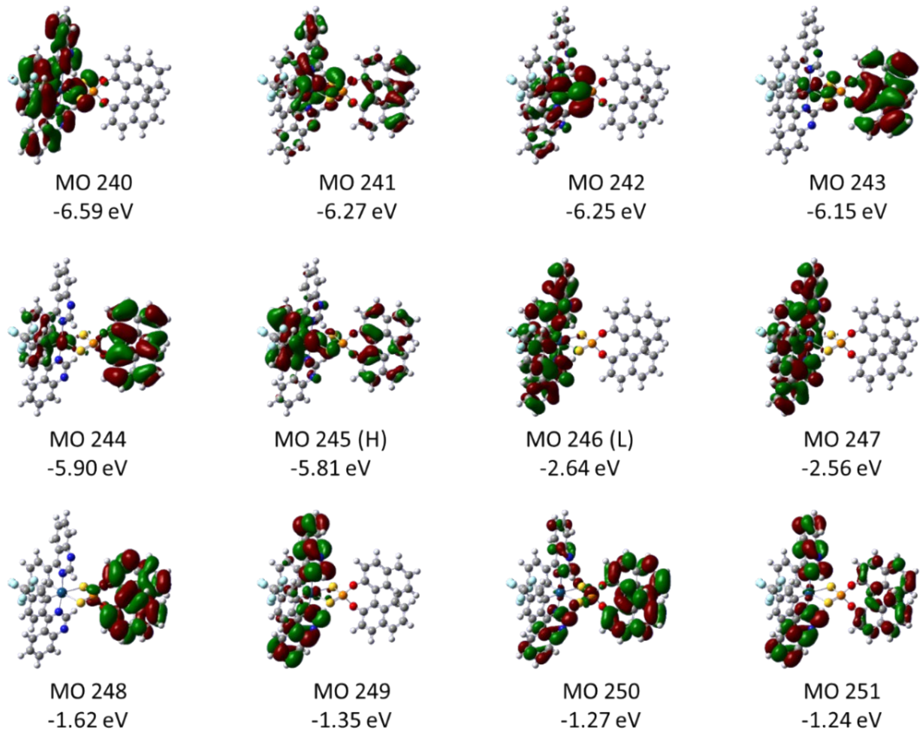

Fig. S25 Electronic clouds distribution of Λ-(tfpqz)$_2$Ir(*S*-**L**$_2$) in selected transitions.

S7. Thermal stability

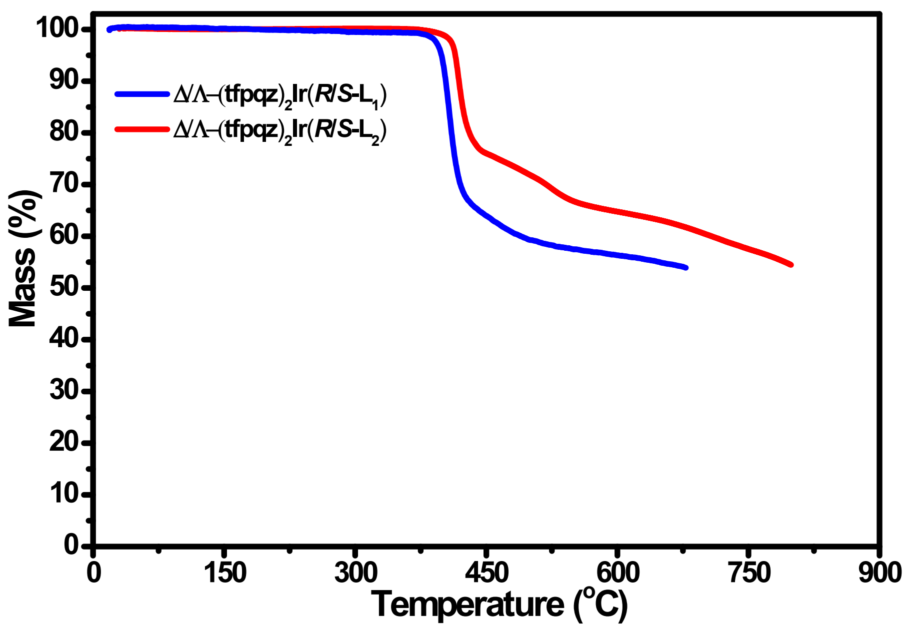

Fig. S26 TGA curves of Δ/Λ-(tfpqz)$_2$Ir(*R/S*-**L**$_1$) and Δ/Λ-(tfpqz)$_2$Ir(*R/S*-**L**$_2$).

S8. Devices fabrication of Δ/Λ-(tfpqz)$_2$Ir(*R*/*S*-L$_1$) and Δ/Λ-(tfpqz)$_2$Ir(*R*/*S*-L$_2$)

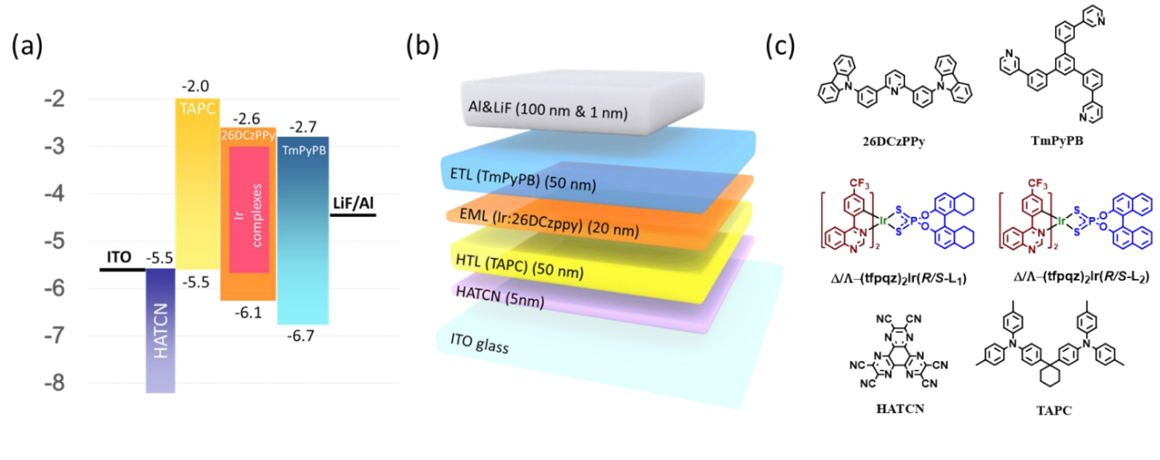

Fig. S27 (a) The schematic energy diagrams of OLED device; (b) Device configuration of OLEDs; (c) Chemical structures of adopted materials.

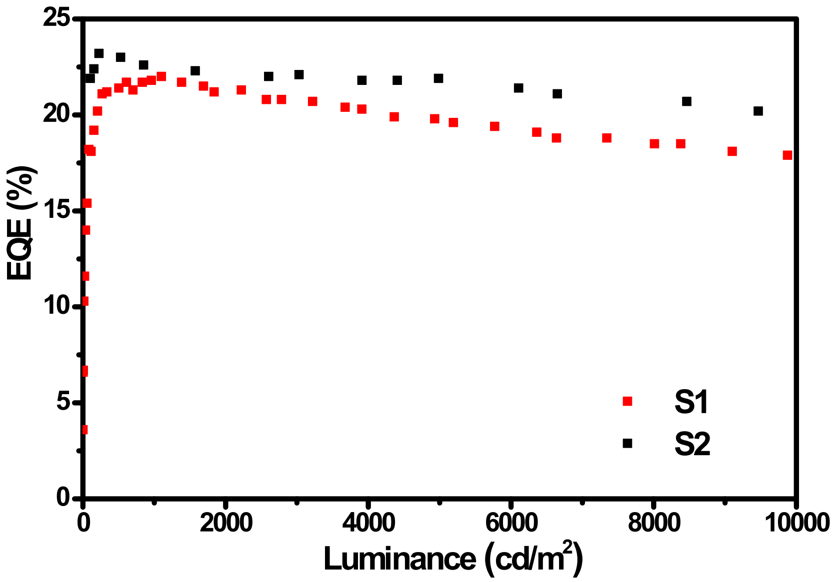

Fig. S28 External quantum efficiency-luminance (*EQE-L*) curves of **S1** and **S2**.

S9. EL color coordinates on CIE (x,y) 1931 chromaticity diagram for devices based on Δ/Λ-(tfpqz)$_2$Ir(*R*/*S*-L$_1$) and Δ/Λ-(tfpqz)$_2$Ir(*R*/*S*-L$_2$)

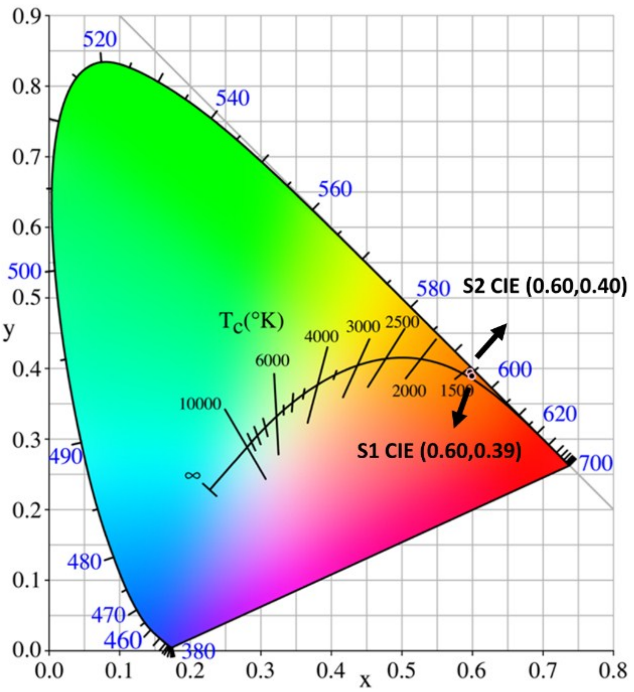

Fig. S29 EL color coordinates on CIE (x,y) 1931 chromaticity diagram for **S1** and **S2**.

S10. Device performance characterization of the CP-OLEDs

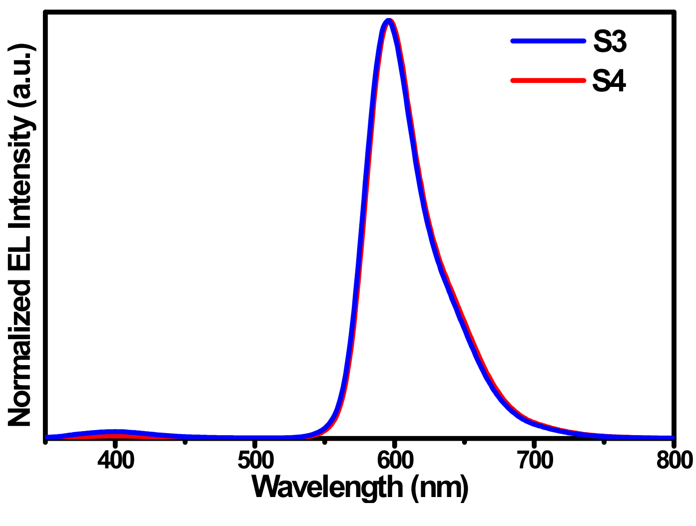

Fig. S30 Normalized EL spectra of **S3** and **S4** at 8 V.

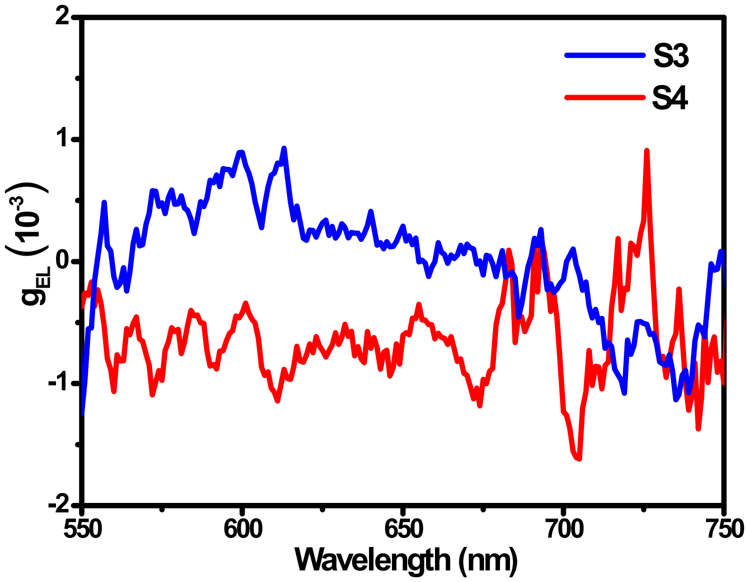

Fig. S31 g_{EL} curves of EL performances of **S3** and **S4**.

S11. References

1. (a) W. Perlikowska, M. Gouygou, M. Mikolajczyk, J. C. Daran, *Asmmetry*, 2004, **15**, 3519-3529; (b) G. Pousse, A. Devineau, V. Dalla, L. Humphreys, M. C. Lasne, J. Rouden, J. Blanchet, *Tetrahedron*, 2009, **65**, 10617-10622; (c) G. Z. Lu, N. Su, H. Q. Yang, Q. Zhu, W. W. Zhang, Y. X. Zheng, L. Zhou, J. L. Zuo, Z. X. Chen, H. J. Zhang, *Chem. Sci.*, 2019, **10**, 3535-3542.